Nano-Processing Techniques Applied in GaN-Based Light-Emitting Devices With Self-Assembly Ni Nano-Masks

Ching-Hua Chiu, Ming-Hua Lo, Tien-Chang Lu, *Member, IEEE*, Peichen Yu, H. W. Huang, Hao-Chung Kuo, *Senior Member, IEEE*, and Shing-Chung Wang, *Life Member, IEEE, Fellow, OSA*

***Abstract*—We have developed a simple method to fabricate nanoscale masks by using self-assembly Ni clusters formed through a rapid thermal annealing (RTA) process. The density and dimensions of the Ni nano-masks could be precisely controlled. The nano-masks were successfully applied to GaN-based light-emitting diodes (LEDs) with nano-roughened surface, GaN nanorods, and GaN-based nanorod LEDs to enhance light output power or change structure properties. The GaN-based LED with nano-roughened surface by Ni nano-masks and excimer laser etching has increased 55% light output at 20 mA when compared to that without the nano-roughened process. The GaN nanorods fabricated by the Ni nano-masks and ICP-RIE dry etching showed 3.5 times over the as-grown sample in photoluminescence (PL) intensity. The GaN-based nanorod LEDs assisted by photo-enhanced chemical (PEC) wet oxidation process were also demonstrated. The electroluminescence (EL) intensity of the GaN-based nanorod LED with PEC was about 1.76 times that of the as-grown LED. The fabrication, structure properties, physical features, and the optical and electrical properties of the fabricated devices will be discussed.**

***Index Terms*—GaN, light-emitting diodes (LEDs), nano-masks, nanorods.**

I. Introduction

DIRECT wide-bandgap gallium nitride (GaN) and other III-nitride-based semiconductors have attracted much attention for potential applications such as blue, green, and ultraviolet (UV) light-emitting diodes (LEDs) and blue laser diodes [1]–[3]. With the rapid development of nano-fabrication technology, fabrication and studies of nanorods in GaN-based semiconductors have attracted considerable interest for potential applications in electronic and optoelectronic devices due to the quantum confinement and the strain relaxation effect [4]. It is also reported that the InGaN/GaN nanorods can exhibit optical and electrical properties that are different from those in the bulk materials.

Manuscript received September 30, 2007; revised January 17, 2008. The work was supported by the MOE ATU program and the National Science Council of the Republic of China under contract NSC95–3114-P-009–001-MY2 and NSC96–2120-M009–006.

The authors are with the Department of Photonics and the Institute of Electro-Optical Engineering, National Chiao Tung University, Hsinchu 300, Taiwan R.O.C. (e-mail: chchiu.eo95g@nctu.edu.tw; minhualo.eo95g@nctu.edu.tw; timtclu@faculty.nCtu.edu.tw; yup@faculty.nctu.edu.tw; hckuo@faculty.nctu.edu.tw; stevinhuang737672@msn.com; scwang@mail.nctu.edu.tw).

Color versions of one or more of the figures in this paper are available online at http://ieeexplore.ieee.org.

Digital Object Identifier 10.1109/JLT.2008.922157

GaN nanorods have been produced by various fabrication methods. In 1997, Han *et al.* first proposed synthesizing GaN nanorods by using carbon nanotubes as templates [5]. The dimension of the synthesized GaN nanorods could be up to 25 μm in length and ranging from 4 to 50 μm in diameter. However, preparing the carbon nanotube is rather complicated. The growth of single-crystal GaN nanorods by hybrid vapor-phase epitaxy [6] has been developed by Kim *et al.*. A mask-free simple process by inductively coupled plasma-reactive ion etching (ICP-RIE) dry etching to fabricate GaN nanorods was proposed by Yu *et al.* [7]. The growth of GaN nanorods by using ferrocene as the catalyst, so-called vapor–liquid–solid (VLS) mechanism, was also demonstrated [8]. Fabrication of GaN nanorods by e-beam patterning and ICP etching was proposed by Chen *et al.* [9]. However, all of these reported methods are relatively complicated. In addition, the typical structures prepared by these methods do not contain active layers, which limit the potential applications for optoelectronic devices.

In this paper, a simple patterning process to produce nanoscale self-assembly Ni islands was proposed. The mean size of the formed Ni nano-islands could be controlled by modifying the initial Ni layer thickness, annealing time, and annealing temperature [10]. The Ni nano-islands formed on top of the GaN-based LED surface could act as nano-masks for excimer laser etching and ICP dry etching since the Ni nano-masks have a good selective etching rate to GaN material. The fabrication process of the Ni nano-mask formation and the key issues to determine the geometry of the formed nano-masks will be described firstly in this report. Then, the Ni nano-masks were used for a surface nano-roughened GaN-based LED by excimer laser etching. The relationship between the surface morphology and the laser fluence will be studied for optimizing the etching condition. The GaN nanorods could also be fabricated by using the self-assembly Ni nano-masks and ICP-RIE etching. The optical properties like temperature-dependent photoluminescence (PL) and time-resolved PL (TRPL) of the nanorods will be studied and discussed. Finally, a novel fabrication process by combining photo-enhanced chemical (PEC) wet oxidation and ICP-RIE process was used to fabricate the GaN-based nanorods LED. The detailed GaN-based LED preparation, fabrication process, and the electroluminescence (EL) characteristics of the fabricated LEDs will also be described in the last part of this paper.

0733-8724/$25.00 © 2008 IEEE

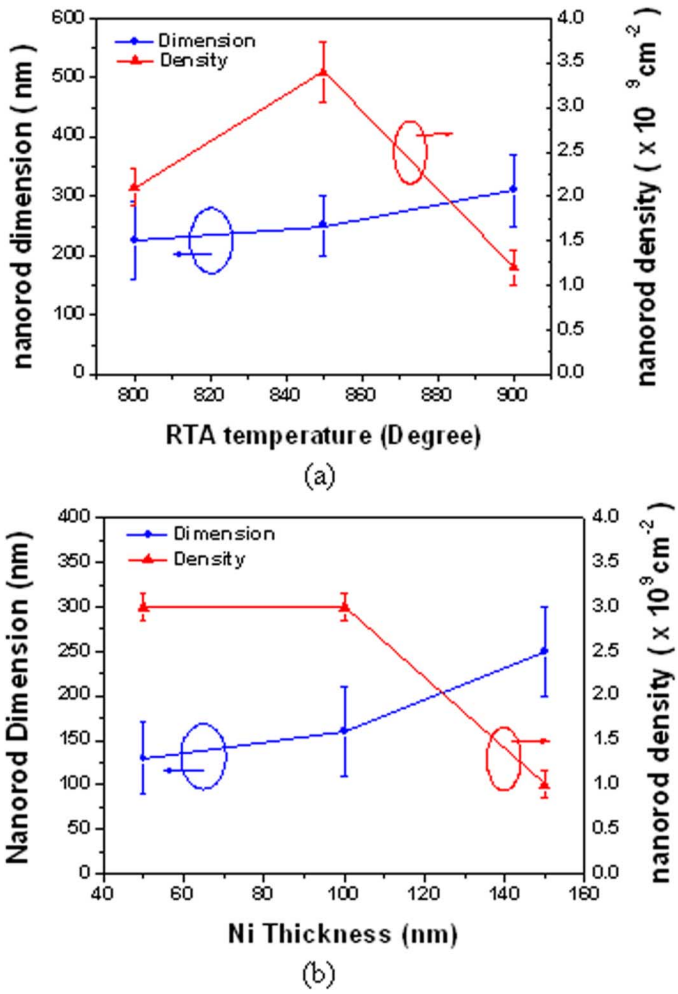

Fig. 1. Mean dimension and density of the formed Ni clusters as a function of the (a) RTA temperature varies from 800 to 900 °C for 1 min and (b) the thickness the initial deposited Ni layer.

II. Ni Nano-Mask Formation

A thin Ni metal layer was first deposited on the surface of a p-GaN layer and subsequently undergone the rapid thermal annealing (RTA) process to form the self-assembly nanometer-sized Ni clusters. Therefore, the formed Ni self-assembly nano-clusters were strongly dependent on the RTA temperature and the thickness of the deposited Ni layer. We estimate the mean dimension and density of the formed Ni clusters as a function of the RTA temperature, and the relationship between the formed clusters and the RTA temperature is shown in Fig. 1. The RTA temperature needs to be chosen above 700 °C to form the self-assembly Ni nano-masks on the epi-surface. Fig. 1(a) shows the nano-masks density can be estimated about 2-3 $\times 10^{9}$ cm^{-2} as the RTA temperatures are within 800 and 900 °C for 1 min at a fixed Ni film thickness of 150 Å. The dimension of the formed Ni nano-masks was ranged from 160 to 380 nm in diameter as the RTA temperature was increased from 800 to 900 °C for 1 min.

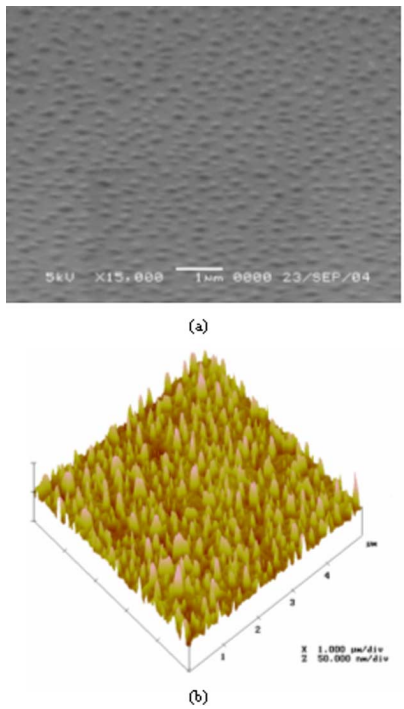

Fig. 2. (a) SEM and (b) AFM images of the Ni nano-mask on p-GaN surface morphology.

The relationship between the formed Ni clusters and the deposited Ni thickness was also estimated. We have examined the effect of initial Ni layer thickness from 50 to 150 Å deposited on the surface of a p-GaN layer at 850 °C RTA process for 1 min. Fig. 1(b) shows the mean dimension and density of the formed Ni nano clusters as a function of the initial Ni layer thickness from 50 to 150 Å. The nanorod densities increased from 1 $\times 10^{9}$ to 3 $\times 10^{9}$ cm^{-2} and the dimension decreased from 250 to 125 nm as the Ni film thickness decreased from 150 to 50 Å. Under the same annealing condition, the Ni cluster became larger and dispersive as the initial Ni thickness was thicker. On the other hand, as the initial Ni thickness decreased, it was easier for Ni migration resulting in a smaller Ni cluster and denser particle matrix at the same annealed condition [11].

Fig. 2 shows the (a) scanning electron microscope (SEM) and (b) atomic force microscope (AFM) images of the Ni nano-mask on p-GaN surface after RTA process. The SEM image in Fig. 2(a) shows that the dimension and density of the self-assembly Ni masks under RTA condition of 750 °C for 1 min were approximately 200 nm and 3 $\times 10^{9}$ cm^{-2}, and the height of the Ni clusters was approximately 30 nm when the original Ni thickness was 100 Å. The AFM image in Fig. 2(b) shows that with the root mean-square (RMS) roughness of the Ni nano-mask is 7.4 nm after RTA process, which is sufficient as etching masks for the subsequent process. One can see the height of the formed Ni nano-masks were nearly one order larger than the initial deposited Ni thickness (from 5 to 30 nm). Thus, stable and durable nanoscale masks for GaN nanorods and LEDs could be achieved by a simple process instead of depositing thick metal or complicated and expensive pattern process and facilities.

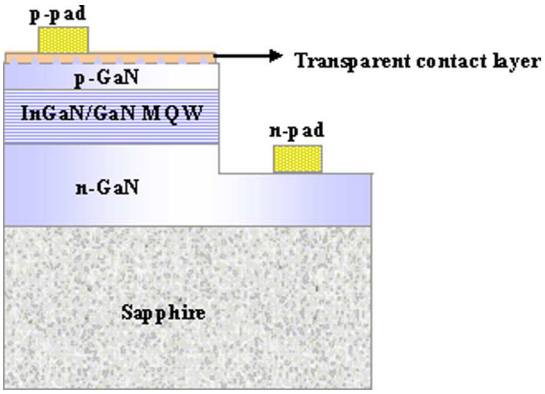

Fig. 3. Schematic diagram of the nano-roughed LED structure.

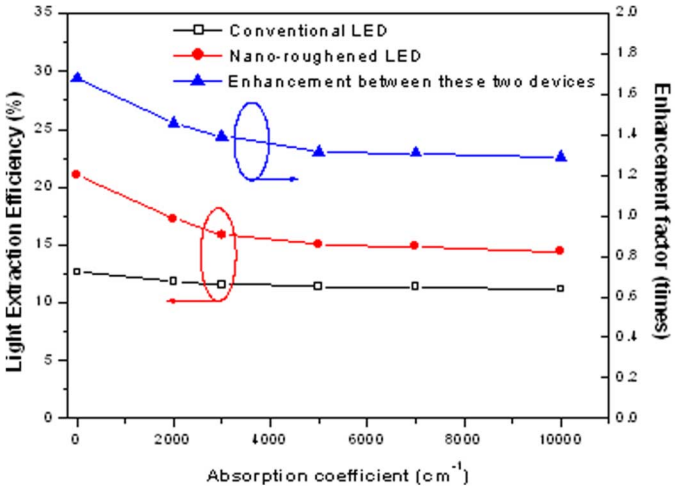

Fig. 4. Simulation describes the light extraction efficiency of LEDs with and without rough top surface as a function of absorption coefficient of the p-GaN.

III. GaN-Based Top-Surface Nano-Roughened LEDs Using Self-Assembly Ni Nano-Masks and Excimer Laser Etching

A. Device Fabrication

Fig. 3 depicts a schematic diagram of the GaN-based LED with nano-roughened surface by Ni self-assembly nano-mask and excimer laser etching. First, we simulated light propagation and reflection using the ray tracing method provided by packaged simulation software Advanced System Analysis Program (ASAP). For simplicity, we employed a two-dimensional model which is similar to GaN-based LED structures. The top mesa area is 300×300 μm^2 and depth is 1 μm with and without rough top surface. Fig. 4 shows light extraction efficiency of conventional, with flat top surface, and rough top surface LED structures as a function of absorption coefficient of the p-GaN layer. The light extraction efficiency here was defined as the ratio of the collected power outside the LED structure and the total power generated from the active region. The result clearly shows that by adding a rough top surface, the extraction efficiency could be greatly enhanced. The extraction efficiency could be enhanced about a factor of 1.29–1.67 times compared with conventional and rough top surface LED structures considering the absorption coefficient of p-GaN layer changed from 10 000 to 100 cm^{-1}.

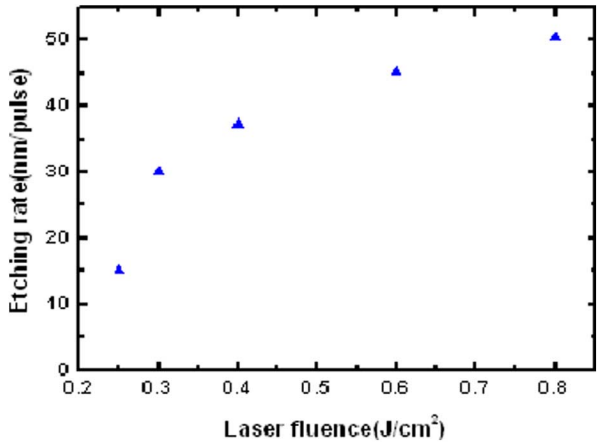

Fig. 5. Etching rate as a function of laser fluence.

The GaN-based LED structures were grown by metal-organic chemical vapor deposition (MOCVD) with a rotating-disk reactor (Emcore $D75^{\mathrm{TM}}$) on a c-axis sapphire (0001) substrate at a growth pressure of 200 mbar.

Trimethylgallium, Trimethylaluminum, ammonia, CP_2Mg and Si_2H_6 were used as sources of Ga, Al, N, Mg, and Si, respectively. The GaN-based LED structure includes a 30-nm-thick GaN low-temperature buffer layer, a 4-μm-thick highly conductive Si-doped GaN layer (grown at 1050 °C), an active region of undoped multiple quantum wells (MQWs) that includes five periods of 2/5-nm-thick $In_{0.21}Ga_{0.79}N$/GaN (grown at 750 °C), a 50-nm-thick Mg-doped AlGaN layer (grown at 1050 °C) and finally a 0.1-μm-thick Mg-doped GaN layer (grown at 1050 °C). The top surface of the GaN-based LED, which is a p-GaN surface, was roughened by the excimer laser etching after the formation of Ni nano-mask on the top surface. The surface roughness of the LED cap layer was measured by the tapping mode AFM (Veeco).

The nano-masks were formed by depositing a Ni thin film with a thickness of 5 nm on a p-GaN surface by electron beam evaporation. RTA was then performed at 750 °C for 1 min to change the Ni layer to the metal Ni nano-masks on the top p-GaN surface as was described in the previous section. Then, a KrF excimer laser at wavelength of 248 nm with a pulsewidth of 25 ns and the incident laser fluence varied from 250 to 800 mJ/cm^2 was used to etch the p-GaN surface in the air atmosphere. In this process, the beam size of KrF laser (1×1 mm^2) was larger than the size of LEDs (300×300 μm^2) to avoid nonuniformity of the laser irradiation on the surface of p-GaN. Fig. 5 shows the etching rate of the p-GaN layer as a function of laser fluence in the air atmosphere. The etching rate increased with the increasing laser fluence. The etching rate of the p-GaN layer from 250 to 800 mJ/cm^2 was determined to be approximately 15 nm/pulse to 50 nm/pulse. After the laser etching process, the nano-roughened LED samples were dipped into hydrochloric acid (HCl) solution for 5 min to remove the residual Ga and Ga oxide on the p-GaN and then dipped into a nitric acid solution (HNO_3) for 5 min to

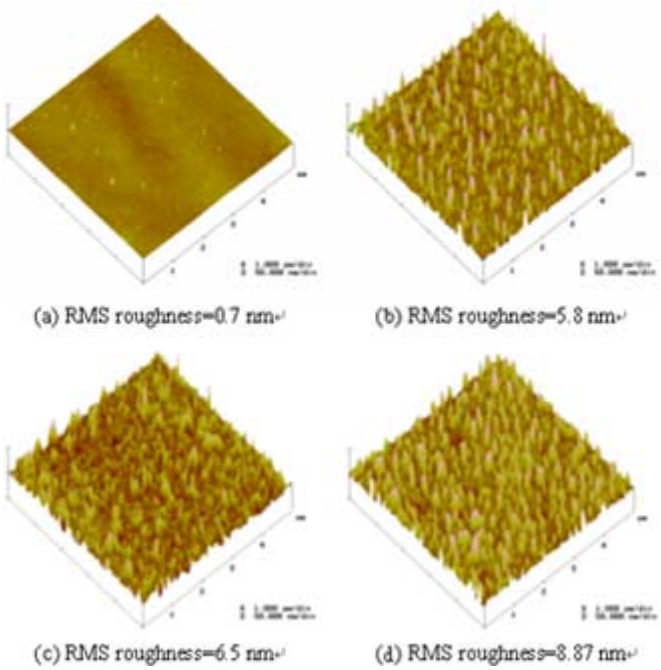

Fig. 6. AFM images of the top surface morphology of a LED sample. (a) Conventional LED p-GaN surface image. Nano-roughened LED top p-GaN surface applied laser etching energy of (b) 300 mJ/cm^2, (c) 400 mJ/cm^2, and (d) 800 mJ/cm^2.

remove the Ni nano-mask from a nano-roughened LED. Afterwards, the GaN-based conventional LED and the LED with a nano-roughened surface were underwent the standard LED fabrication process.

Fig. 6 shows the AFM figures of the surfaces of the GaN-based LEDs with different laser fluence. Fig. 6(a) shows that the conventional p-GaN cap has a RMS roughness of 0.7 nm, and a surface depth of approximately 2 nm, demonstrating a rather smooth p-GaN surface in the conventional LED. Fig. 6(b)–(d) shows the AFM images of the p-GaN surface roughened by the laser etching energy of 300, 400, and 800 mJ/cm^2, respectively. The RMS roughness of p-GaN surface increased drastically from 5.8 to 8.7 nm as the energy of excimer laser increased from 300 to 800 mJ/cm^2.

B. Characteristics of the Surface Nano-Roughened LED

The current-voltage (*I–V*) characteristics of the conventional and nano-roughened LEDs were also measured and plotted in Fig. 7. The forward voltages of the conventional and nano-roughened LEDs etched by the laser energy of 300 mJ/cm^2 were 3.54 and 3.27 V at a driving current of 20 mA, respectively. Furthermore, the dynamic resistance ($R = dV/dI$) of the nano-roughened LED (27 Ω) was 32% lower than that of the conventional LED (40 Ω). The results indicated that the nano-roughening surfaces could facilitate the p-type contact to form an Ohmic contact with a low specific resistance when the laser etching fluence ranged from 250 to 400 mJ/cm^2. However, when the laser etching fluence is over 600 mJ/cm^2, the laser etching process could result in a Schottky contact with a high specific resistance, which might be due to the fact that the surface morphology was too rough to form good contacts on the top p-GaN surface.

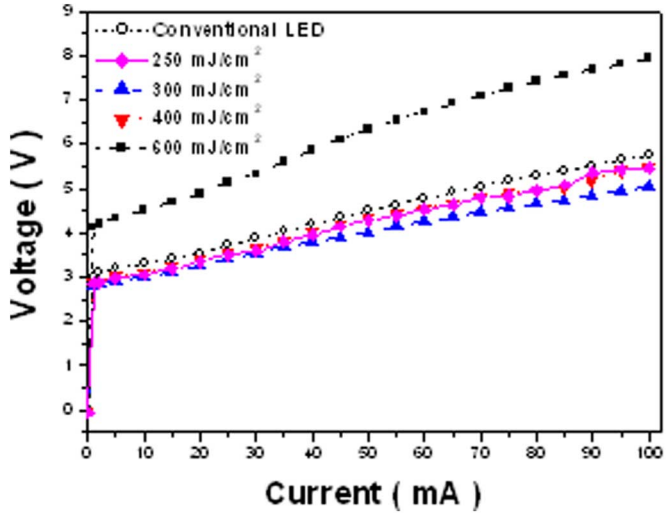

Fig. 7. Forward *I–V* curves of conventional and nano-roughened LEDs.

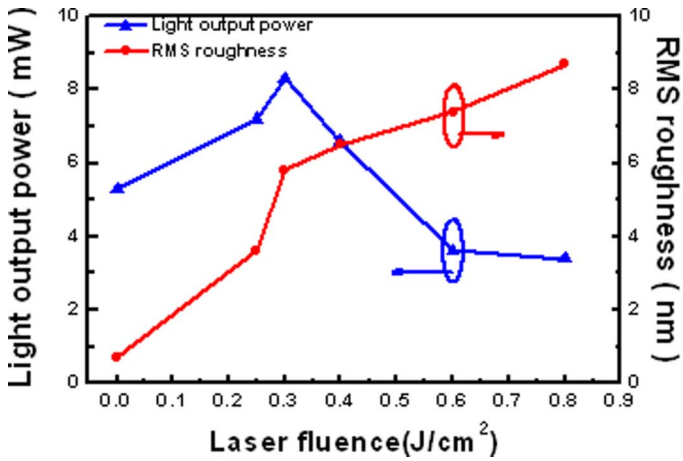

Fig. 8. Light output power versus RMS surface roughness characteristics of conventional and nano-roughened LEDs.

The EL property of the nano-roughened GaN-based LED was measured by injecting a continuous current into a chip device at room temperature. The light output was detected using a calibrated large-area Si photodiode placed 5 mm from the top of the device. This detecting condition covers almost all of the power emitted from the top of the LEDs. Fig. 8 shows the intensity–current (*L–I*) characteristics versus the RMS roughness of the surfaces in nano-roughened LEDs. Nano-roughening the p-GaN surface with the laser etching energy of 300 mJ/cm^2 increased the output power of the conventional GaN-based LEDs by a factor of 1.55. The enhancement of the wall-plug efficiency of the nano-roughened LEDs over the conventional LED was 68% at a driving current of 20 mA. The nano-roughened LEDs with energy of laser etching over 600 mJ/cm^2 shows slightly lower light output than the conventional LED. This could be due to a Schottky contact with a high specific resistance (as shown in Fig. 7) and generation of nonradiative defects and slight deterioration in the InGaN/GaN MQW active regions during the high-energy laser etching [12]. The RMS roughness of the nano-roughed surface morphology was increase from 0.7 to 8.4 nm as the laser fluence increased from 0 to 800 mJ/cm^2.

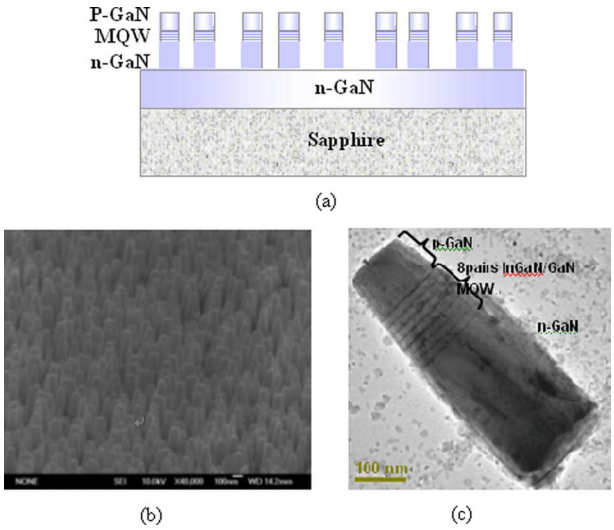

Fig. 9. (a) Schematic diagram of $In_{0.3}Ga_{0.7}N$/GaN MQWs green nanorods structure. (b) Tilted 45° SEM, and (c) TEM images of $In_{0.3}Ga_{0.7}N$/GaN MQWs green nanorods.

IV. $In_{0.3}Ga_{0.7}N$/GaN Green Emission Nanorods

The formed Ni nano-masks were then used for fabricating GaN nanorods. By combining the ICP-RIE process and the self-assembly nano-masks, the GaN nanorods with controllable dimension and density could be achieved. In this section, we present the results of enhanced emission intensity properties of InGaN/GaN MQW green nanorods and analyze the dominant enhancement mechanism using temperature dependent PL and TRPL.

A. Nanorods Formation

The samples for nanorods were grown by MOCVD and the structure consists of a 50-nm-thick GaN nucleation layer, a 3-μm-thick Si-doped n-GaN buffer layer, an unintentionally doped $In_{0.3}Ga_{0.7}N$/GaN MQW active region, and a 0.1-μm-thick Mg-doped p-GaN. The MQW active region consists of eight periods of 7/15-nm-thick $In_{0.3}Ga_{0.7}N$/GaN well layers and barrier layers. The grown sample was then deposited a Ni thin film with a thickness of 50 Å on a p-GaN surface by electron beam evaporation. RTA was then performed at 750 °C for 1 min to form Ni nano-masks on the top p-GaN surface. Then, the LED samples were etched down to the n-type GaN layer by the ICP-RIE system (SAMCO ICP-RIE 101iPH) operated at 13.56 MHz under a gas mixture of $Cl_2/Ar = 50/20$ sccm with 2 min of etching time to form nanorods. The ICP source power, bias power and the chamber pressure of the ICP-RIE system were set at 400/100 W. Then, the samples were dipped into a nitric HNO_3 at 100 °C for 5 min to remove the Ni nano-masks. Details of the nanorod formation process were given in [10]. A schematic diagram of fabricated $In_{0.3}Ga_{0.7}N$/GaN MQWs nanorods is shown in Fig. 9(a). Fig. 9(b) and (c) shows the tilted 45° SEM image and transmission electron microscope (TEM, JEOL, JEM-200CX) image of the fabricated $In_{0.3}Ga_{0.7}N$/GaN MQWs nanorods, respectively. The dimension and density of the nanorods were estimated from the SEM image to be around 130 nm and 3×10^9 cm^{-2}, respectively. The etching depth estimated from the TEM image is about 0.6 μm. In Fig. 9(c), eight pairs of $In_{0.3}Ga_{0.7}N$/GaN MQWs of 7/15-nm-thick $In_{0.3}Ga_{0.7}N$/GaN well layers and barrier layers embedded within the nanorod can be clearly observed.

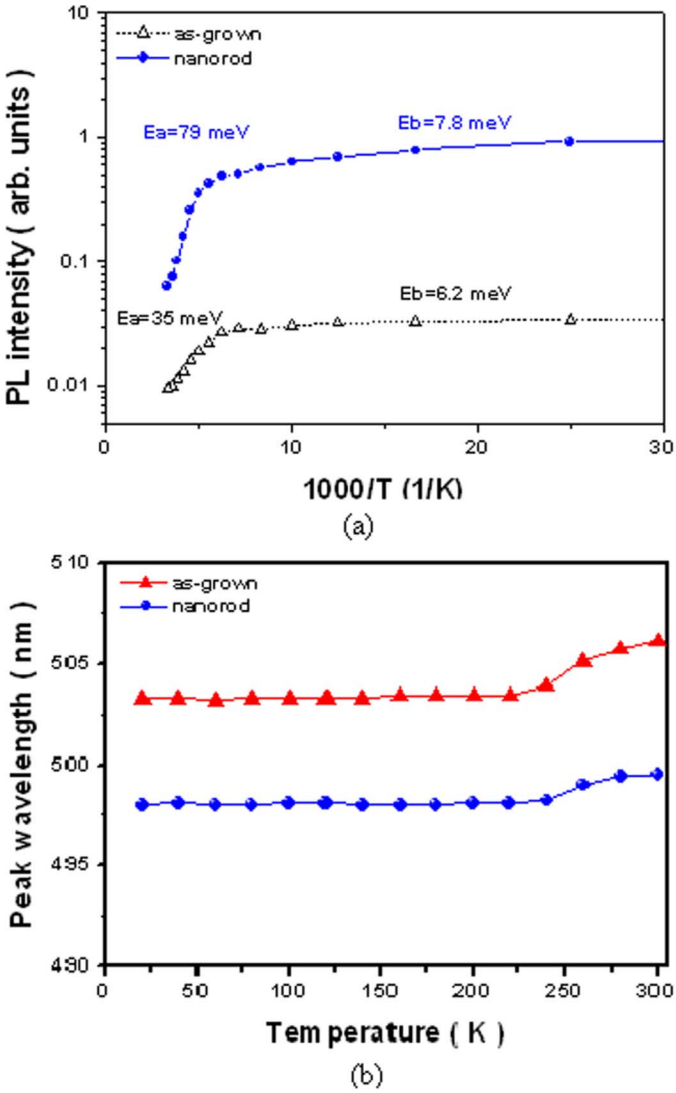

Fig. 10. (a) Arrhenius plot of an integrated PL intensity obtained from the $In_{0.3}Ga_{0.7}N$/GaN MQWs active layer emission over a temperature range from 20 to 300 K. (b) Comparing the PL spectra from as-grown and green nanorods of excited by a 325-nm He–Cd laser from 20 to 300 K.

B. Temperature-Dependent Pl of Nanorods

The PL properties of the GaN nanorods were studied at temperatures between 20 and 300 K. For the PL measurement, the GaN nanorod samples were excited by a 325-nm He–Cd laser with an excitation power of 25 mW, and the emitted luminescence light was collected through a 0.32-m spectrometer with a charge-coupled device (CCD) detector. The focused spot size of the He–Cd laser was estimated to be about 200 μm in diameter. Fig. 10(a) shows the Arrhenius plot of an integrated PL intensity obtained from the $In_{0.3}Ga_{0.7}N$/GaN MQWs active layer emission for the as-grown and GaN nanorod samples over a temperature range from 20 to 300 K. The PL intensity in the GaN nanorods is enhanced by a factor of approximately

3.5 over the as-grown sample emission at room temperature as shown in Fig. 10(a). The large emission enhancement could result from improvement either in internal quantum efficiency or external extraction efficiency. The temperature-dependent PL results in Fig. 10(a) could be fitted with the following formula: $I_T = I_0/[1 + \mathrm{A}\exp(-E_\mathrm{a}/kT) + \mathrm{B}\exp(-E_\mathrm{b}/kT)]$, where the I_T, I_0 are integrated PL intensity for T and 0 K, A and B are constant, k is Boltzmann constant, T is temperature, and E_a is the activation energy for PL quenching, and E_b is generally associated to the free exciton binding energy [13]. The energy E_b of as-grown and nanorods were approximately 6.2 and 7.8 meV, which was similar to the previous report [14]. However, the activation energy E_a of as-grown and nanorod samples were 35 and 79 meV, respectively. Though the high surface ratio around the peripheral of the nanorods could provide many nonradiative recombination paths, the larger activation energy of the GaN nanorod structure we obtained still demonstrated higher potential barriers for carriers easily localized in the effective potential minima in the GaN nanorod structures [15].

Fig. 10(b) compares the PL peak emission energy of the as-grown sample and GaN nanorod samples measured from 20 to 300 K. The PL emission peak of as-grown and nanorod samples are 503.3 and 498 nm at a temperature of 20 K and 506.1 nm and 499.5 nm at room temperature, respectively. A blue-shift of the emission peaks from the GaN nanorods in comparison to the as-grown samples could be observed. Since the 100-nm diameter of the nanorod is too large to result in the quantum confinement effect, the blue-shift of the nanorod emission peak from that of the as-grown sample could be caused by the partial reduction of the piezoelectric (PZ) field in the nanorod. The blue-shift of 6.6 nm (32.5 meV) at the temperature of 300 K corresponds to the reduction in the piezoelectric field caused by the partial strain release; the reduction of the internal field in a quantum well was obtained to be around 32.5 mV/7 nm $=$ 0.05 MV $\cdot$ cm^{-1}, where 7 nm is the well thickness. A larger wavelength red-shift of as-grown samples, 2.8 nm (13.6 meV), than that of the nanorod samples, 1.5 nm (7.4 meV), was clearly observed as the temperature increased from 20 to 300 K, indicating that possible strain relaxation occurred in the GaN nanorod samples. Therefore, the reduction of the internal PZ field could account for part of the reasons for the blue-shift of the PL emission peak.

C. TRPL of Nanorods

The TRPL measurements were carried out using a second-harmonic pulsed Ti:sapphire laser at a wavelength of 400 nm and a time-correlated single photon counting detection system. The power density of the pumped beam in the TRPL measurement was about 1 kW $\cdot$ cm^{-2}. Fig. 11 shows the carrier lifetime from the as-grown and GaN nanorod samples measured by TRPL at 10 and 300 K, respectively. Since a purely radiative recombination at $T = 10$ K can be assumed [16], the radiative lifetime of the GaN nanorod sample is similar to that of the as-grown sample, which is approximately 54 ns, indicating that the radiative recombination process for both samples is similar and the internal field reduction in the GaN nanorods sample plays a minimal role in the emission enhancement. As the temperature increased to 300 K, the carrier lifetimes were further shortened to 8.7 and 16.5 ns for the GaN nanorod and as-grown samples due to the increase of the non-radiative recombination rate in the GaN nanorod structures. The relatively larger non-radiative recombination rate at room temperature for the GaN nanorod sample was probably due to the increasing surface recombination around the periphery of the GaN nanorod. Generally, reduction of the internal PZ field facilitates a better wavefunction overlapping of electrons and holes in the $In_{0.3}Ga_{0.7}N$/GaN MQWs that could result in the increase of the emission efficiency and enhancement in the PL emission intensity of the nanorods. However, the TRPL measurement results reveal that the reduction of the internal PZ field could not be large enough to enhance the radiative recombination process in the green GaN nanorods consisted MQWs with high In content and a relatively large QW thickness. As a result, the internal quantum efficiency of the GaN nanorod sample at room temperature could not be improved, indicating that the PL intensity enhancement observed from the GaN nanorod sample could result mainly from the increased emission surface of the GaN nanorod structure.

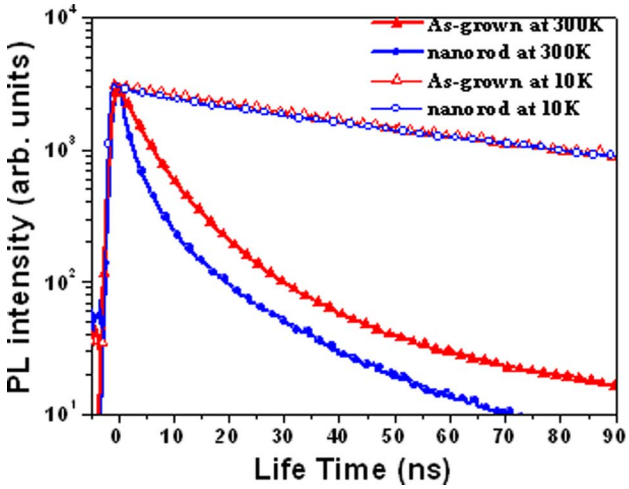

Fig. 11. TRPL life time curves of the $In_{0.3}Ga_{0.7}N$/GaN MQW as-grown and green nanorod samples for the main InGaN emission peak measured at 10 and 300 K.

V. GaN-Based Nanorod LEDs Using PEC Oxidation Process

After nanorods with InGaN/GaN MQWs was fabricated and a large enhancement of the PL intensity was observed, it is expectable to fabricate the GaN-based nanorod LED with high light output efficiency. However, the rough unprotected sidewalls of MQWs embedded in nanorods etched by ICP-RIE could suffer from a large leakage current, resulting in poor electrical properties. In addition, nanorods fabricated via such methods are difficult to form p-type ohmic contacts for each individual nanorod. In the meantime, the photo-enhanced chemical (PEC) wet oxidation process has been used in GaN-based LEDs to oxidize the exposed surface material for passivation and surface roughening [17]. Thus, we introduce a novel method combining the PEC wet oxidation and GaN nanorod process to fabricate GaN-based nanorod LEDs.

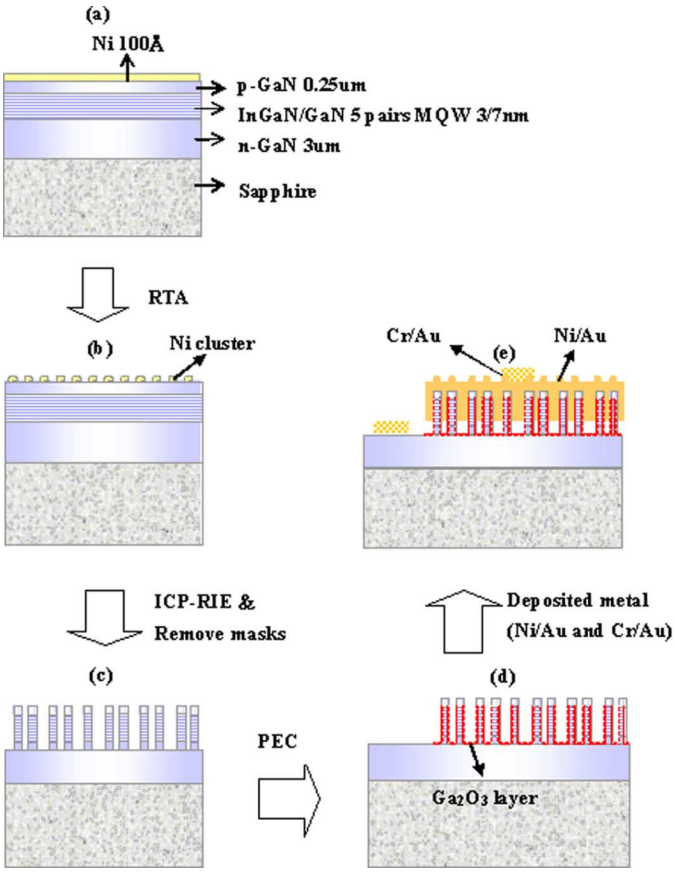

Fig. 12. Schematic illustration of GaN-based nanorods LED process flowchart. (a) Thin Ni layer deposited on LED surface. (b) Ni clusters were formed on surface after 850 °C RTA. (c) ICP-RIE process to fabricate GaN nanorods and then remove the Ni clusters in heated HNO_3. (d) Ga_2hboxO_3 layer was formed on the exposed surface by PEC wet oxidation process. (e) Contact metal of Ni/Au was deposited on nanorods to form connections with the p-type ohmic contacts.

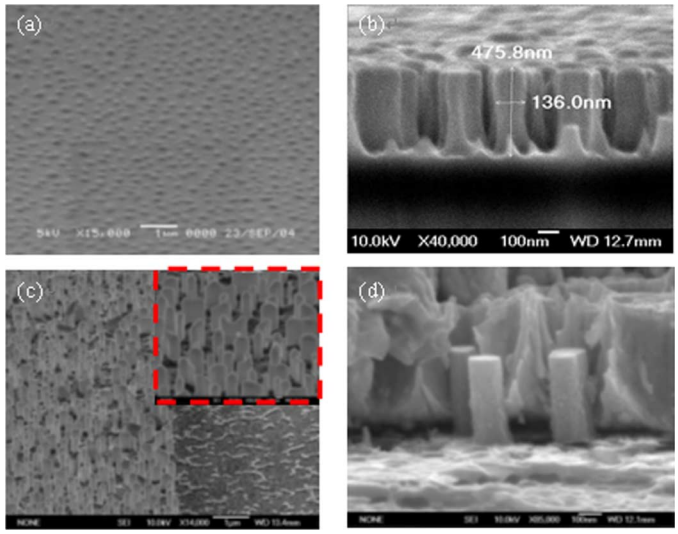

Fig. 13. SEM images of (a) Ni nano-masks on p-GaN top surface after RTA process and (b) GaN-based nanorods LED after ICP-RIE etching. (c) GaN-based nanorods LED after PEC process. (d) GaN-based nanorods LED after deposited contact metal.

A. Device Fabrication

The process flowchart for making the GaN-based nanorod LEDs with the PEC oxidation process is shown in Fig. 12. The GaN-based LED samples were grown by MOCVD on a c-axis sapphire (0001) substrate; they consist of a 50-nm-thick GaN nucleation buffer layer, a 3.0-μm-thick highly conductive Si-doped GaN layer, five periods of 3/7-nm-thick undoped $In_{0.21}Ga_{0.79}N$/GaN MQWs, a 50-nm-thick Mg-doped AlGaN layer, and finally a 0.25-μm-thick Mg-doped GaN layer. The as-grown samples were then sent for the nanorod fabrication process. First, a 100 Å Ni layer was deposited on top of the LED samples by an E-gun evaporator [Fig. 12(a)]. The Ni-coated LED samples were subsequently subjected to RTA under flowing N_2 at 850 °C for 1 min to form self-assembly Ni nano-masks [Fig. 12(b)]. Then, the LED samples were etched down to the n-type GaN layer by the ICP-RIE to form nanorods. Then, the samples were dipped into a HNO_3 at 100 °C for 5 min to remove the Ni nano-mask [Fig. 12(c)] and was followed by the PEC oxidation process. An 800-W Hg lamp was used as the illumination source in the PEC oxidation process in the unstirred deionized water. An external dc bias fixed at positive 20 V was applied to the n-type GaN layer surface as the anode contact and platinum was used as the cathode, with 10 min as the exposure time. The light power density of the Hg lamp was fixed at 2.5 W $\cdot$ cm^{-2} to illuminate the front side of the LED samples. Then, the Ga_2O_3 layer was formed at the nanorod sidewall and the ICP-etched n-type GaN layer [Fig. 12(d)]. The p-type layer was nearly unoxidized due to its low conductivity [18]. Finally, a 20/500-nm-thick Ni/Au layer was deposited on the entire surface of the GaN-based nanorod LED to form a connection with the p-type ohmic contacts for an individual nanorod. A 20/800-nm-thick Cr/Au was then deposited as the p and n bonding electrodes [Fig. 12(e)].

After all processes of the nanorod LEDs were done, the dimensions and density of the GaN-based nanorod LED samples with and without the PEC oxidation process were estimated by SEM images, as shown in Fig. 13. Fig. 13(a) shows that the size and density of the self-assembly Ni nano-masks on the p-GaN surface of an LED sample were approximately 150 nm and 3×10^9 cm^{-2}. The InGaN/GaN MQW nanorod density was estimated to be approximately 3×10^9 cm^{-2}. Fig. 13(b) shows that the diameter and the etching depth of nanorods were about 140 nm and 0.5 μm, respectively. Fig. 13(c) shows the GaN-based nanorod LED after the PEC process; the left-hand side shows the nanorods made with the PEC process and the right-hand side shows the ICP-RIE etching surface after the PEC process. The inset of Fig. 13(c) framed with a red dashed line shows higher magnification of the nanorods after the PEC oxidation process. Compared with the size of the GaN nanorods in Fig. 13(b) and (c), the diameters of the GaN nanorods made without and with the PEC oxidation process were about 140 and 155 nm, respectively. Fig. 13(d) shows the Ni/Au contact metal deposited on GaN nanorods to form connections with the p-type ohmic contacts for each individual nanorod.

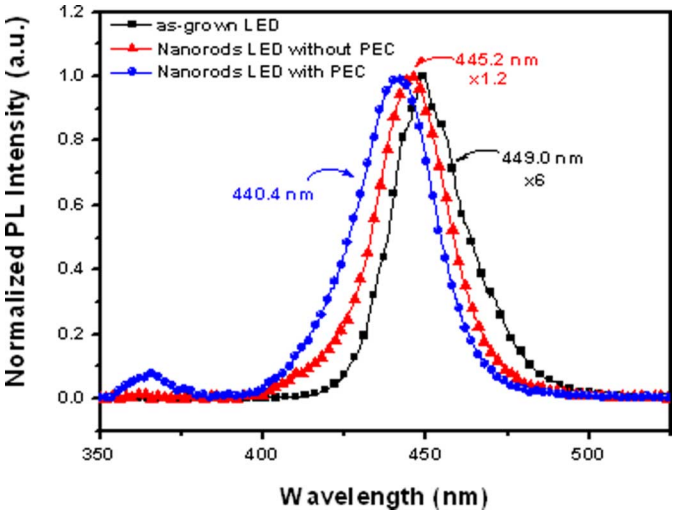

Fig. 14. Normalized PL intensity spectra for as-grown LED and GaN-based nanorods LED with and without PEC at room temperature.

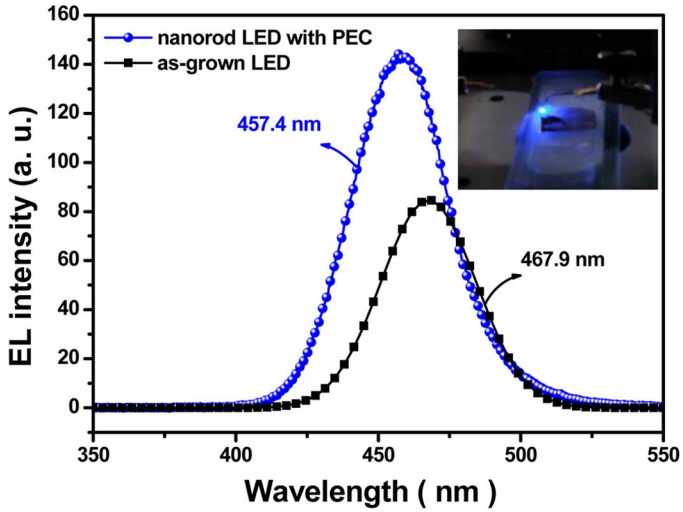

Fig. 15. EL intensity spectra for as-grown LED and GaN-based nanorods LED with PEC at room temperature. The inset shows the photograph image of a blue emission from GaN-based nanorods LED at 1 mA dc current.

B. PL Characteristics of the LEDs

Fig. 14 shows the normalized PL spectrum of the as-grown LED sample, GaN-based nanorods LED samples with and without PEC process measured at room temperature. He–Cd laser (325 nm) was used with an excitation power of 25 mW and the power density of 1.5 W/cm. The PL emission peaks of the InGaN/GaN active layer were observed at 449.0, 445.2, and 440.4 nm for as-grown samples, and GaN-based nanorods samples without and with PEC oxidation process, respectively. The PL peak intensities of InGaN/GaN MQW active layers in nanorods with and without the PEC oxidation process were enhanced by factors of approximately six and five times compared with as-grown LED samples. The blue-shift phenomena were observed both at the nanorods LED samples with and without the PEC oxidation process, and the blue-shift values were 3.8 nm (20 meV) and 8.6 nm (50 meV), respectively. The blue-shift might be caused by the partial reduction of the piezoelectric field by the strain release in the nanorods structures [19]. The blue-shift phenomenon of nanorods with PEC was stronger than that of without PEC due to the further reduced diameters. The peak shifts can be translated to the reduction of the piezoelectric field at around 20 meV/3 nm = 66.7 kV/cm and 50 meV/3 nm = 166.7 kV/cm, for GaN-base nanorod LED samples with and without PEC oxidation process, respectively (where 3 nm is the well thickness). From the PL results, one can see that the nanorods with the PEC oxidation process have a higher PL intensity and a larger piezoelectric reduction due to the smaller nanorods diameters by the PEC oxidation process. It shows that the PEC oxidation process not only can form an oxidation layer to isolate the individual nanorod electrically, also reduce the diameter of the nanorods for a stronger strain relaxation effect.

C. EL Characteristics of the LEDs

Fig. 15 shows the room-temperature EL spectrum of the as-grown LED and GaN-based nanorods LED samples with the PEC oxidation process at an injection current of 1 mA.

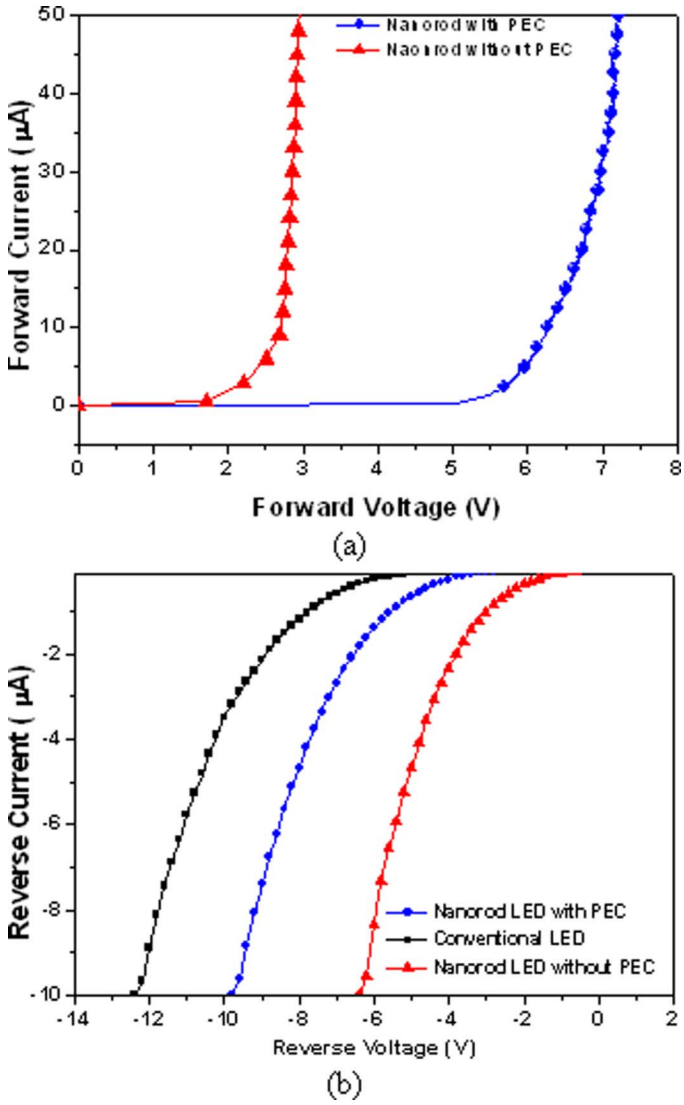

Fig. 16. (a) Reverse-bias and (b) forward-bias *I–V* characteristics of the GaN nanorods made with and without the PEC oxidation process.

The inset of Fig. 15 shows the emission image of the InGaN/GaN MQW nanorods LED. It shows that the PEC oxidation process can effectively form oxidation layers to isolate nanorods and facilitate contact formation. The EL intensity of nanorods LED with PEC was about 1.76 times that of as-grown LED. The EL emission peaks were observed at 467.9 and 457.4 nm for as-grown samples and GaN-based nanorods samples with the PEC oxidation process, respectively. The blue-shift effect was again observed at the nanorods LED samples with PEC oxidation process with the blue-shift value of 10.5 nm (60 meV), which was similar to the observation in the PL measurement.

The reverse-bias and forward-bias *I–V* characteristics of nanorods made with and without the PEC oxidation process were also measured, and they are shown in Fig. 16(a) and (b). *The reverse current under –5 V were* -0.08, -0.64, and -4.65 μA *for conventional, nanorods with PEC and nanorods without PEC LEDs, respectively.* The reverse-bias leakage current in the nanorods made with the PEC oxidation process is significantly reduced compared to that in the nanorods made without the PEC oxidation process. This is due primarily to the fact that oxidation layers produced in the PEC oxidation process form excellent isolation layers to reduce the leakage current through the sidewalls of the nanorods. In addition, the forward-bias characteristics also show a difference in current level for the two types of nanorod LEDs. A higher turn-on voltage of the PEC-oxidized nanorod LED was clearly observed. Such high forward voltage is probably due to the smaller contact area and the nonoptimized ohmic contact metal conditions. The accompanying thermal effect also explained why the enhancement factor in the EL result was smaller than that in PL result.

VI. Conclusion

The self-assembly Ni nano-masks with controllable size formed by RTA process have been successfully applied in surface nano-roughened GaN-based LED, GaN nanorods and GaN-based nanorod LEDs and all have shown superior characteristics over their counterparts fabricated by conventional methods. The dimension and density of the formed Ni nano-masks could be controlled by modifying the initial Ni thickness and RTA temperature. The GaN-based LED with nano-roughened surface by Ni nano-masks and excimer laser etching with laser fluence of 300 mJ/cm^2 has increased 55% light output at 20 mA when compared with that without the nano-roughened process. The operating voltage of the surface nano-roughened LED was reduced from 3.54 to 3.27 V at 20 mA, and the series resistance was reduced by 32%. The GaN nanorods were also fabricated by the self-assembly nano-masks and ICP-RIE dry etching. An increase in the PL emission intensity of the GaN nanorod by 3.5 times over that of the as-grown sample was measured. A blue-shift of 32.5 meV in the GaN nanorod PL emission peak from that of the as-grown sample was observed and attributed to a partial reduction of the piezoelectric field. A novel fabrication process by combining PEC and GaN nanorods were demonstrated to realize GaN-based nanorod LED. The EL spectrum with a more efficient and 10.5 nm blue-shift peak was observed from the GaN-based nanorods LED made with the PEC process in comparison with that of the as-grown LED sample.

Acknowledgment

The authors would like to thank J. R. Chen, Dr. Y. A. Chang, and C. C. Kao of National Chaio Tung University for their helpful suggestions.

References

[1] S. Nakamura, M. Senoh, S. Nagahama, N. Iwasa, T. Yamada, T. Matsushita, H. Kiyoku, and Y. Sugimoto, "InGaN-based multi-quantum-well-structure laser diodes," *Jpn. J. Appl. Phys.*, vol. 35, pp. L74–L76, 1996.

[2] S. Nakamura, T. Mokia, and M. Senoh, "Candela-class high-brightness InGaN/AlGaN double-heterostructure blue-light-emitting diodes," *Appl. Phys. Lett.*, vol. 64, pp. 1687–1689, 1994.

[3] N. Lizuka, K. Kaneko, N. Suzuki, T. Asano, S. Noda, and O. Wada, "Ultrafast intersubband relaxation (< 150 fs) in AlGaN/GaN multiple quantum wells," *Appl. Phys. Lett.*, vol. 77, pp. 648–650, 2000.

[4] T. H. Hsueh, H. W. Huang, C. C. Kao, Y. H. Chang, M. C. Ou-Yang, H. C. Kuo, and S. C. Wang, "Characterization of InGaN/GaN multiple quantum well nanorods fabricated by plasma etching with self-assembled nickel metal nanomasks," *Jpn. J. Appl. Phys.*, vol. 44, pp. 2661–2663, 2005.

[5] W. Q. Han, S. S. Fan, Q. Q. Li, and Y. D. Hu, "Synthesis of gallium nitride nanorods through a carbon nanotube-confined reaction," *Science*, vol. 277, pp. 1287–1289, 1997.

[6] H. M. Kim, D. S. Kim, T. W. Kang, Y. H. Cho, and K. S. Chung, "Growth and characterization of single-crystal GaN nanorods by hydride vapor phase epitaxy," *Appl. Phys. Lett.*, vol. 81, pp. 2193–2195, 2002.

[7] C. C. Yu, C. F. Chu, J. Y. Tsai, H. W. Huang, T. H. Hsueh, C. F. Lin, and S. C. Wang, "Gallium nitride nanorods fabricated by inductively coupled plasma reactive ion etching," *Jpn. J. Appl. Phys.*, vol. 41, pp. L910–L912, 2002.

[8] W. Q. Han and A. Zettl, "Pyrolysis approach to the synthesis of gallium nitride nanorods," *Appl. Phys. Lett.*, vol. 80, pp. 303–305, 2002.

[9] H. S. Chen, D. M. Yeh, Y. C. Lu, C. Y. Chen, C. F. Huang, T. Y. Tang, C. C. Yang, C. S. Wu, and C. D. Chen, "Strain relaxation and quantum confinement in InGaN/GaN nanoposts," *Nanotechnology*, vol. 17, pp. 1454–1458, 2006.

[10] H. W. Huang, C. C. Kao, T. H. Hsueh, C. C. Yu, C. F. Lin, J. T. Chu, H. C. Kuo, and S. C. Wang, "Fabrication of GaN-based nanorod light emitting diodes using self-assemble nickel nano-mask and inductively coupled plasma reactive ion etching," *Mater. Sci. Eng. B*, vol. 113, pp. 125–129, 2004.

[11] J. D. Carey, L. L. Ong, and S. R. P. Silva, "Formation of low-temperature self-organized nanoscale nickel metal islands," *Nanotechnology*, vol. 14, pp. 1223–1227, 2003.

[12] C. J. Youn, T. S. Jeong, M. S. Han, J. W. Yang, K. Y. Lim, and H. W. Yu, "Influence of various activation temperatures on the optical degradation of Mg doped InGaN/GaN MQW blue LEDs," *J. Cryst. Grow.*, vol. 250, pp. 331–338, 2003.

[13] C. C. Yu, C. F. Chu, J. Y. Tsai, C. F. Lin, and S. C. Wang, "Electrical and optical properties of beryllium-implanted Mg-doped GaN," *J. Appl. Phys.*, vol. 92, pp. 1881–1887, 2002.

[14] Y. L. Lai, C. P. Liu, Y. H. Lin, R. M. Lin, D. Y. Lyu, Z. X. Peng, and T. Y. Lin, "Effects of the material polarity on the green emission properties of InGaN/GaN multiple quantum wells," *Appl. Phys. Lett.*, vol. 89, pp. 151906–151908, 2006.

[15] Y. H. Cho, S. K. Lee, H. S. Kwack, J. Y. Kim, K. S. Lim, H. M. Kim, T. W. Kang, S. N. Lee, M. S. Seon, O. H. Nam, and Y. J. Park, "Carrier loss and luminescence degradation in green-light-emitting InGaN quantum wells with micron-scale indium clusters," *Appl. Phys. Lett.*, vol. 83, pp. 2578–2580, 2003.

[16] E. Deleporte, J. M. Martinez, A. Filoramo, D. Batovski, Roussignol, C. Delalande, C. Morhain, E. Tourni'e, and J. P. Faurie, "Time-resolved photoluminescence and steady-state optical investigations of a Zn/sub 1-x/Cd/sub x/Se/ZnSe quantum well," *Nuovo Cimento*, vol. 17D, pp. 1435–1440, 1995.

[17] C. F. Lin, J. H. Zheng, Z. J. Yang, J. J. Dai, D. Y. Lin, C. Y. Chang, Z. X. Lai, and C. S. Hong, "High-efficiency InGaN-based light-emitting diodes with nanoporous GaN:Mg structure," *Appl. Phys. Lett.*, vol. 88, pp. 083121–083121, 2006.

[18] C. F. Lin, Z. J. Yang, J. H. Zheng, and J. J. Dai, "Enhanced light output in nitride-based light-emitting diodes by roughening the mesa sidewall," *IEEE Photon. Technol. Lett.*, vol. 17, no. 10, pp. 2038–2040, Oct. 2005.

[19] H. W. Huang, J. T. Chu, T. H. Hsueh, M. C. Ou-Yang, H. C. Kuo, and S. C. Wang, "Fabrication and photoluminescence of InGaN-based nanorods fabricated by plasma etching with nanoscale nickel metal islands," *J. Vac. Sci. Technol. B*, vol. 24, pp. 1909–1912, 2006.

Ching-Hua Chiu received the B.S. and M.S. degree in power mechanical engineering from National Tsing Hua University, Taiwan, R.O.C., in 2004 and 2006, respectively. He is currently working towards the Ph.D. degree in the Department of Photonics at Chiao Tung University, Taiwan, R.O.C.

His current research is focused on the vertical LED and high-performance GaN-based LED via nanotechnology.

Ming-Hua Lo received the B.S. and M.S. degrees in physics from Chung Yuan Christian University, Taiwan, R.O.C., in 2004 and 2006, respectively.

His research interests include III–V compound materials grown by MOCVD, quantum structure materials, light emission diode, and solar cell.

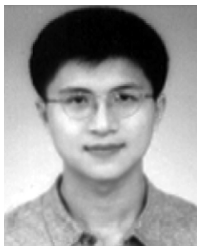

Tien-Chang Lu (M'07) received the B.S. degree in electrical engineering from National Taiwan University, Taiwan, R.O.C., in 1995, the M.S. degree in electrical engineering from the University of Southern Los Angeles, in 1998, and the Ph.D. degree in electrical engineering and computer science from National Chiao Tung University, Taiwan, R.O.C., in 2004.

He joined the National Chiao Tung University as a faculty member of Department of Photonics in August 2005.

Peichen Yu received the B.S. degree in electrophysics and the M.S. degree in electrooptical engineering from National Chiao-Tung University, Taiwan, R.O.C., in 1996 and 1998, respectively, and the Ph.D. degree in electrical engineering from the University of MichiGaN, Ann Arbor, in 2004.

She worked as a Design Engineer for the Advanced Design group of Intel Corporation, Hillsboro, OR, for two years. Her main responsibilities were OPC-related design rule definition and OPC algorithm development of the diffusion layer for the CMOS 65- and 45-nm nodes. She joined the Department of Photonics, National Chiao-Tung University, as an Assistant Professor in August 2006. Her current research interests include the design and development of photonic crystal-based and quantum dot-based semiconductor devices

H. W. Huang was born in Tainan, Taiwan, R.O.C., in 1977. He received the B.S. degree from the Department of Physics from Tamkang University, Taipei, Taiwan, R.O.C., in 2000 and the M.S. and Ph.D. degrees from the Institute of Electro-Optical Engineering, National Chiao Tung University (NCTU), Hsinchu, Taiwan, R.O.C., in 2002 and 2007.

He joined Mesophotonics Limited, Hsinchu, Taiwan, R.O.C. in 2007 as a Senior Engineer of the R&D Department. His research interests include GaN-based optical and electrical nano-structure devices.

Hao-Chung Kuo (M'98–SM'06) received the B.S. degree in physics from National Taiwan University, Taiwan, R.O.C., the M.S. degree in electrical and computer engineering from Rutgers University, New Brunswick, NJ, in 1995, and the Ph.D. degree from the Electrical and Computer Engineering Department, University of Illinois at Urbana Champaign, in 1999.

He has an extensive professional career both in research and industrial research institutions that includes Research Consultant in Lucent Technologies, Bell Laboratories (1993–1995); a Senior Research Engineer at Filtronic Solid State (1999–2000); and a Member of Technical Staff in Fiber-Optics Division at Agilent Technologies (2000–2001), and LuxNet Corporation (2001–2002). Since October 2002, he has been with the National Chiao Tung University, Hsinchu, Taiwan, R.O.C., as a Faculty Member of the Institute of Electro-Optical Engineering. His current research interests include semiconductor lasers, VCSELs, blue and UV LED lasers, quantum-confined optoelectronic structures, optoelectronic materials, and high-speed semiconductor devices. He has authored and coauthored 80 internal journal papers and four granted patents.

Dr. Kuo is a member of The International Society for Optical Engineers (SPIE) and the MRS.

Shing-Chung Wang (M'79–SM'03–LM'07) received the B.S. degree from National Taiwan University, Taiwan, R.O.C., the M.S. degree from National Tohoku University, Sendai, Japan, and the Ph.D. degree from Stanford University, Stanford, CA, in 1971, all in electrical engineering.

He has an extensive professional career both in academic and industrial research institutions that includes a faculty member at National Chiao Tung University (1965–1967); a Research Associate at Stanford University (1971–1974); a Senior Research Scientist at Xerox Corporation (1974–1985); and a Consulting Scientist at Lockheed-Martin Palo Alto Research Laboratories (1985–1995). In 1995, he rejoined National Chiao Tung University, Taiwan, R.O.C., as a faculty member of Institute of Electro-Optical Engineering.

Prof. Wang is a Fellow of the Optical Society of America (OSA) and a recipient of Outstanding Scholar Award from the Foundation for the Advancement of Outstanding Scholarship.